ChemComm

REVIEW ARTICLE

View Article Online
View Journal



Cite this: DOI: 10.1039/d5cc07296d

# Nanoclusters formed by gas-phase condensation and their size-dependent properties

Xiaoyi Guan, Wenyu Gao and Kam Tong Leung *

The study of nanoclusters (NCs) has provided invaluable insights into the interactions among small assemblies of atoms, where their size encapsulates vital information about atom–atom synergies that govern morphology, defects, and electronic states. The precise tuning of NC size has become a pivotal factor in optimizing their performance. Evolving in tandem with other ultra-high vacuum (UHV) techniques over recent decades, the gas-phase condensation technique has emerged as a remarkable approach to synthesize solvent-free and ligand-free NCs with tailored size distributions. This review provides a dual focus on the formation and size control of NCs through the gas-phase condensation technique, elucidating its advantages and limitations primarily through the use of magnetron-based sputtering sources, as well as on the size-dependent physical, chemical and electronic properties of NCs in their diverse applications. The capacity to engineer NCs with precision down to the number of atoms has ushered in a new era of transformative impacts on chemistry, materials science, and beyond. The precise control of NC size and composition has opened new opportunities for tailoring their size-specific properties for specific applications, thereby harnessing their full potential to meet the grand challenges of the rapidly evolving world of nanotechnology.

Received 23rd December 2025,
Accepted 25th February 2026

DOI: 10.1039/d5cc07296d

rsc.li/chemcomm



## 1. Introduction: nanoclusters

Nanoclusters (NCs) are aggregates of atoms and molecules that are typically smaller than a few tens of nanometers in size.[1–3] In this special size regime, the electronic structure retains distinct individual states instead of merging into bands. Compared to their bulk materials, NCs exhibit not only different electronic structures, but also a significantly higher surface area-to-volume ratio (or specific surface area), specific to their sizes. These size-dependent properties drive development of novel approaches to new material discovery and manipulation. Currently, there is a large variety of NCs that can be generated from metals and metal oxides along with their mixtures. Given their unique properties, these NCs find important industrial applications in catalysis,[4,5] biomedicine,[6,7] energy,[8] sensing,[9–12] and electronics.[13,14] These applications are closely linked to the small size of the NCs, which provide high specific surface areas and more active sites for interaction with the surrounding medium. Additionally, changes in their electronic

*WATLab and Department of Chemistry, University of Waterloo, 200 University Ave. W., Waterloo, Ontario, N2L 3G1, Canada. E-mail: tong@uwaterloo.ca*

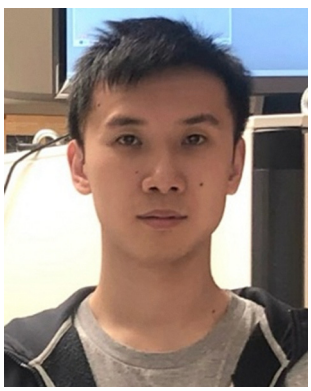

**Xiaoyi Guan**

*Xiaoyi Guan is a post-doctoral research fellow at the University of Waterloo, and completed his PhD in the Nanotechnology program at the same university in 2024. His research interests include nanoclusters and their applications in photoelectrochemical water splitting and special magnetic properties. He also works on fabricating novel memristor devices and developing new techniques involving advanced ion beam lithography.*

**Wenyu Gao**

*Wenyu Gao obtained her PhD in the Nanotechnology program in 2024 and is currently a post-doctoral research fellow at the University of Waterloo. Her research includes the development of nanomaterials for chemical sensing and photoelectrochemical hydrogen generation. Her recent work involves synthesis of bimetallic catalysts for multipurpose reactions.*

structures introduce novel reactivity, sensitivity, and selectivity. The inherent phenomenon of quantum confinement in these NCs leads to discrete electronic states, allowing for precise control over their optical and electronic properties by size manipulation. In particular, transition metal oxide NCs often exhibit a range of defect states that result in multiple oxidation states and mid-gap states within the clusters of different sizes. The presence of mid-gap states and the availability of diverse structures composed of ordered arrays and assemblies make these materials promising candidates for use as catalysts in photoelectrochemical water splitting and $CO_2$ reduction,[15] and as active components in various sensors.[10,16–18] More importantly, these defect-rich transition metal oxide NCs could also manifest in novel phases that are not readily observable at room temperature. These new (metastable) phases could exhibit other fascinating properties, such as ferromagnetism, not found in stable bulk phases.[2] In short, the size of the NCs is critical to unlocking the evolution of electronic structures and other hidden characteristics, while offering deep insights into the mechanisms that connect the properties of the bulk phase with the atomic domain. This size-dependent perspective is crucial for understanding how changes at the nanoscale could influence the overall behavior and yet-to-explore capabilities of materials.

A well-known ''bottom-up'' strategy of synthesizing NCs involves building NCs from atoms and molecules with precise size selection and manipulation in order to achieve better control over their structures and functionalities.[19] To date, there have been many methods for synthesizing metal and metal oxide NCs, including hydrothermal methods,[20] self-assembly,[13] wet-chemistry impregnation methods,[15] and gas-phase condensation.[2,4,21] With over 30 years of development, gas-phase condensation (also known as gas-phase aggregation and cluster beam technique) now offers significant advantages over other methods of NC synthesis.[22] This technique provides high flexibility in material selection and the capability to incorporate multiple targets simultaneously in one condensation chamber. Utilizing a DC or RF magnetron sputtering source, this method can generate NCs of most solid metals and metal oxides, especially those with high melting points, given appropriate sputtering targets.[23–25] More importantly, gas-phase condensation can be used to synthesize NCs without the use of solvents, ligands, or linkers, thereby ensuring that the products are free of contaminants. This stands in marked contrast to wet-chemistry and hydrothermal methods that often involve more complex operations and procedures. The gas-phase condensation technique also allows for more precise tuning of both size and composition of the NCs. In-flight modifications, coatings, and characterization can also be easily integrated into the process, providing enhanced control over the properties of the NCs.[26] Additionally, this technique is compatible with any type of substrate that can withstand low-vacuum conditions, and substrate preparation is relatively less time-consuming. Overall, gas-phase aggregation is a highly versatile and efficient method, and is ideal for producing NCs with tunable size and tailored functionalities for diverse applications. In this review, we focus on two interconnected aspects: (1) the magnetron sputtering-based gas-phase condensation technique with post-synthesis size selection, and (2) the size-dependent properties of the resulting NCs. Together, these topics provide a comprehensive overview for understanding and advancing the application of size-selected NCs.

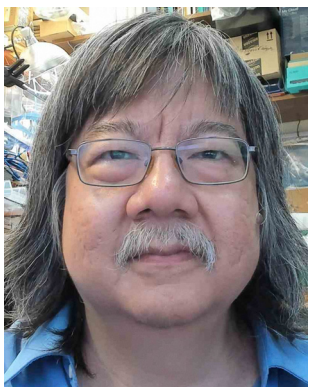

**Kam Tong Leung**

*Kam Tong Leung received his PhD from the University of British Columbia in 1984. He is currently a Professor of Chemistry at the University of Waterloo and the founding director of the Waterloo Advanced Technology Laboratory (WATLab). His current research interests focus on the fabrication of low-dimensional nanomaterials including nanoclusters, nanoparticles, and nanowires using novel methods and their applications in catalysis, biosensing, green energy and nanoelectronics.*

## 2. Gas-phase condensation technique

Employed since the 1980s to synthesize NCs, the gas-phase condensation technique generally involves two vacuum chambers: a condensation chamber and a deposition chamber, linked by differential pumping that creates a pressure gradient.[27] In the condensation chamber, the target material is vaporized by an energy or particle beam. The gaseous atoms or molecules are then carried through the water or liquid nitrogen cooled condensation chamber by a buffer gas, typically argon or helium, following the pressure gradient. Here, the gas-phase target atoms collide with one another and the buffer gas atoms, losing thermal energy, and condense into NCs. These NCs then exit through an aperture into the deposition chamber, where they are deposited onto substrates. With the explosive development of ultrahigh vacuum techniques and nanotechnologies in the past decades, gas-phase condensation has become more advanced, and it is now capable of generating a wide variety of novel NCs. Nonetheless, this technique still consists of the following three basic steps:[2,28] target evaporation, condensation, and deposition.

As the first step of the gas-phase condensation technique, evaporation of the target material involves converting the (solid) target material into the gas phase. High vacuum conditions are required to ensure that the gas-phase target remains of high purity. Fig. 1 summarizes several common methods for evaporating the target materials, including the seeded supersonic nozzle source, thermal gas aggregation, sputtering source, pulsed arc cluster ion source, and laser ablation source.[29] The seeded supersonic nozzle source has the

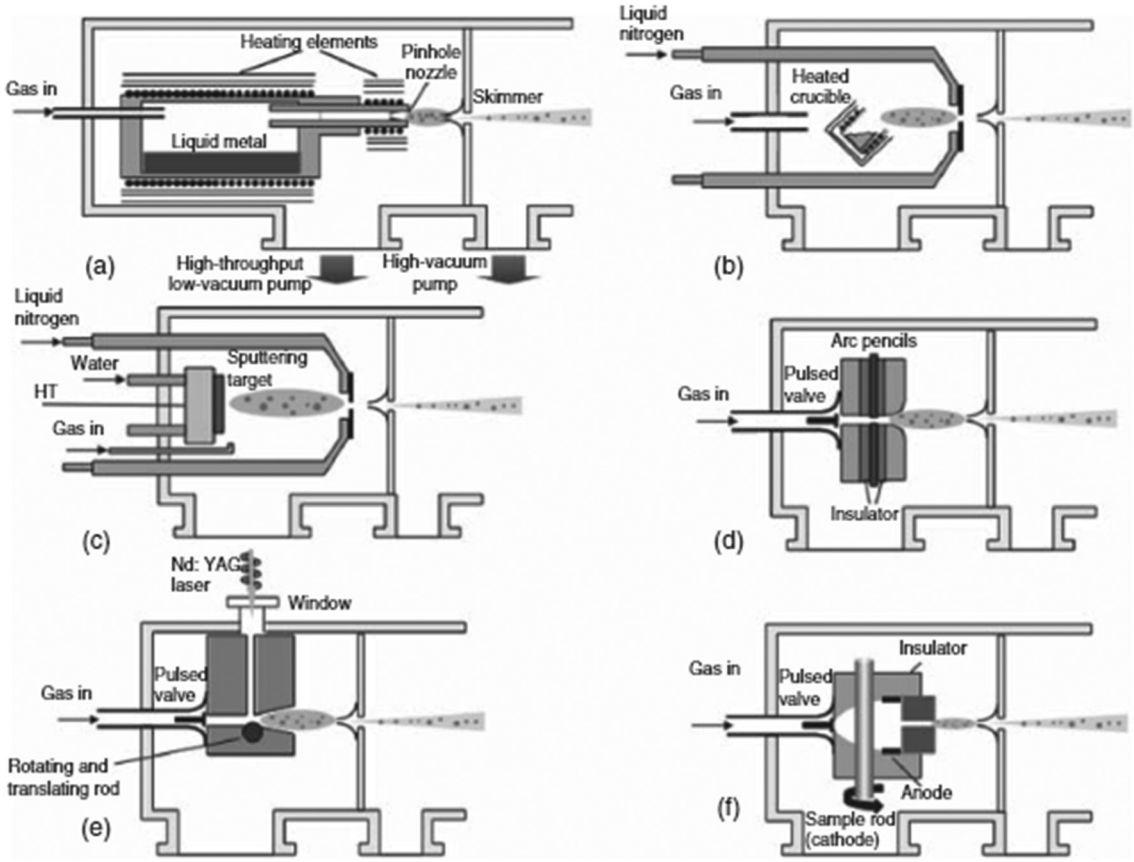


Fig. 1 Basic layouts of common sources employed for the gas-phase condensation technique: (a) seeded supersonic source: the vapor of a target material with a low melting point is carried by a high-pressure inert gas into a condensation chamber, while the sudden expansion of the gas rapidly cools the target vapor to cause condensation into clusters; (b) thermal evaporation source: a heated crucible is used to evaporate the target for further cluster condensation; (c) sputtering source: a magnetron sputtering source is used to generate the target gas vapor; (d) pulsed-arc cluster ion source: the evaporated plume is produced by a pulsed arc coinciding with the gas burst; (e) laser ablation source: a Nd-YAG laser pulse focused onto the target is used to vaporize the target material; and (f) microplasma cluster source: a pulse of high pressure inert carrier gas is introduced to promote the sputtering yield. Reproduced with permission from ref. 29. Copyright 2008, Elsevier.

advantage of producing a high flux NC beam, but it is not compatible for targets with high melting points. While the laser ablation source has the flexibility of target selection, it also introduces complexity into the system. On the other hand, the sputtering source, especially the magnetron-based sputtering source, has been widely used for generating gaseous materials from solids by particle beam collision, and it has been considered as the most promising source due to its flexible selection of a wide range of targets, ease of operation, and ability to finely tune the gas-phase target generation rate.[30] By simply adding more magnetron sputtering sources with different targets, this technique provides a powerful and versatile solution to create a wide variety of multi-component NCs.[25,31] By sequencing each sputtering source on and off individually with different time intervals, bi-metallic (A + B) or alloy (AB) NCs can be easily synthesized from just two sources (for metal A and metal B). Huttel *et al.* have also demonstrated that different core–shell structures can be precisely realized by controlling the position of each sputtering source (*i.e.*, each source has its own aggregation length).[27] Clearly, NCs with ternary, quaternary, quinary compositions and beyond with various core–shell and other combinatorial structures can in principle be obtained by adding more sources.[27,31–34]

The condensation of clusters is the most critical step in NC synthesis, because it enables controlling the ultimate size and structure of the NCs. This process involves the formation of seeds near the target region, followed by their aggregation into NCs. Fig. 1 illustrates the necessity of an aperture along a pressure gradient to effectively condense gas-phase target germs into clusters. Computational fluid dynamics simulations have demonstrated that differential pumping from behind the aperture can create a suitable pressure gradient and direct the flow of the carrier gas, enhancing the condensation process.[35] Additionally, an inert gas, typically argon, is introduced not only to effect sputtering of the target material but also to aid in the formation of these initial seeds.[36] The formation and growth of the NCs by gas-phase condensation involve the following simplified mechanism, shown schematically in Fig. 2a using the synthesis of size-selected $ZrO_2$ NCs as the example:

$$M + M + Ar + Ar^+ + e^- \rightarrow M_2^- + Ar^+ + Ar \quad \text{(seed formation)}$$

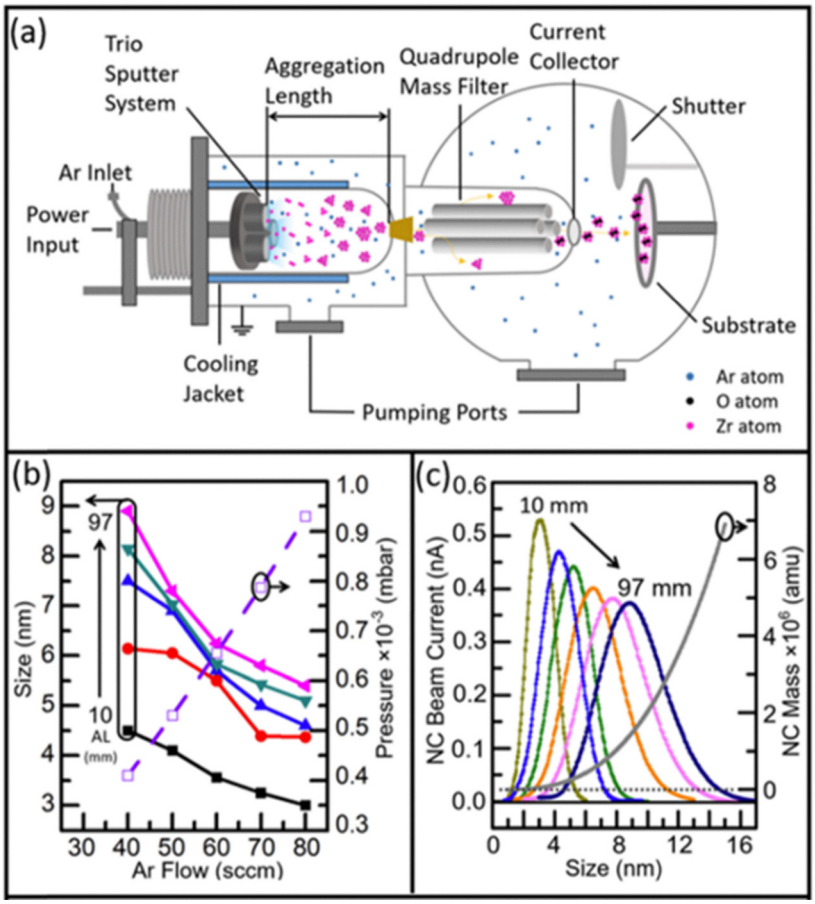


Fig. 2 (a) Schematic representation of the Nanogen NC deposition system for producing a size-selected NC beam, which involves (i) generation of free atoms by DC magnetron sputtering, (ii) seed formation by collision and atom aggregation into bigger clusters, and (iii) beam collimation *via* a 3 mm diameter entrance aperture and size selection of the NCs by a quadrupole mass filter. (b) Mode size (in diameter, left axis) of Zr NCs and the deposition chamber pressure (right axis) as a function of Ar flow rate (from 40 to 80 sccm in steps of 10 sccm) for selected aggregation lengths (AL = 10, 30, 50, 70, and 97 mm). The mode cluster size corresponds to the size (diameter) of the maximum in the cluster size distribution. (c) Zr NC size distribution, as reflected by the beam current obtained at the collector of the quadrupole mass filter, for a fixed Ar flow rate (30 sccm) and selected ALs (10, 30, 50, 70, 90, and 97 mm), along with the mass of Zr NCs (right axis) for selected NC sizes. Reproduced with permission from ref. 2. Copyright 2020, American Chemistry Society.

$$M_m^- + M \rightarrow M_{m+1}^- \quad \text{(aggregation)}$$

$$M_m^- + \text{substrate} \rightarrow M_m(\text{ad}) + \text{substrate} + e^- \quad \text{(landing and neutralization)}$$

where Ar is the buffer gas, $M_m$ ($m$ = 2, 3, …, $n$) is a free metal cluster species, and $M_m$(ad) is a metal cluster adspecies on the substrate.

Intense research has been directed towards understanding the growth mechanism of NCs within the condensation zone, encompassing facets of nucleation and transport. This field of investigation can be categorized into two principal types of studies. The first category employs molecular dynamics to simulate the interactions between gas-phase atoms during collisions, yielding highly accurate pictures of NC growth.[37–39] Based on this atomistic approach, Monte Carlo simulations have focussed solely on pre-defined system transitions rather than the comprehensive trajectories of every individual particle.[24,40,41] The second category of studies harnesses computational fluid dynamics to model the flow and transport of NCs within the condensation zone.[35,42,43] In particular, these latter studies probe the effect of the gas flow rate and the positioning of the sputtering source, while examining such important variables as the distance between the source and the exit aperture, commonly referred as the aggregation length. Both types of inquiries, *via* molecular dynamics and computational fluid dynamics, have yielded noteworthy results. Indeed, these investigations emphasize the critical roles played by the pressure within the condensation chamber and the flow rate of the carrier gas. As these factors fundamentally influence the dwell time of nanoscale aggregates, they significantly affect the ultimate variations in the size distributions of the NCs.

Manipulating the condensation process is key to synthesizing NCs with different sizes, phases, and oxidation states. Several parameters can be adjusted to fine-tune the NC condensation, including the argon (Ar) gas flow rate, aggregation length (AL, defined as the distance between the target and the exit aperture), and cooling temperature of the condensation

 

zone. The Ar flow rate and aggregation length are the two most important parameters, which work together to change the dwell time and, thus, the NC size distribution.[2,4,43] As illustrated in Fig. 2c, a longer AL promotes a longer dwell time, resulting in a bigger NC mode size and a wider distribution. On the other hand, Fig. 2b presents the resulting NC mode size from a combination of Ar flow rate and the aggregation length, as an example of Zr NC synthesis. For a fixed aggregation length, such as 10 mm, an Ar flow rate of 80 sccm produces more sputtering, more seed formation, and shorter dwell time, which results in a very small mode size of 3 nm. Tuning NC size distribution is especially important because it also maximizes the deposition efficiency when the NC beam passes through the mass filter. Although lowering the temperature of the condensation zone is more challenging than manipulating other parameters, water or liquid nitrogen has been effectively used to cool the chamber walls of the condensation (also called aggregation) zone, which could significantly impact the lattice structure of the NC due to the cooling rate.[35] Furthermore, simultaneously introducing some reactive gases, such as $O_2$ and $H_2O$, into the condensation zone can alter the oxidation state or aggregation status of the NCs. Indeed, introducing oxygen through a leak valve is a commonly used method to modify the oxidation state of transition metal oxide NCs, such as $TiO_x$.[44] Zhao *et al.* demonstrated that introducing water vapor into the condensation germs acted as an adhesive component to form core–satellite Au NC complexes.[45] Alternatively, introducing helium (He) as an inert carrier gas could significantly increase the gas flow speed inside the aggregation region, resulting in a narrower NC size distribution with a smaller mode size. However, too much He may prevent seed formation and result in the dilution of sputtering atoms and low NC beam current.[28]

The NCs carried out from the condensation chamber by the buffer gas are ready for deposition. The NC beam can in principle be deposited onto any vacuum-compatible substrate.[23] However, if a thick NC film is required, conductive substrates are preferred in order to prevent charging from the negatively charged NCs. Additionally, the final NC deposition can be modified by applying a sample bias to control the landing energetics and/or changing the substrate temperature during the deposition process (*e.g.*, *in situ* annealing).[31,46] The application of substrate bias can alter the kinetic energy upon which the NCs land on the substrate, which is a particularly important parameter given the inherent charge of the NCs. This variation in the landing energy strongly affects the ultimate morphology of the NCs deposited on the substrate.[47] This is supported by Langevin molecular dynamics simulations, which show that upon reaching the substrate with distinct kinetic energies, the ensuing impact energy could elevate the NC temperature significantly, reaching thousands of Kelvin.[48] Depending on the substrate bias, the NCs could consequently undergo structural deformation and re-crystallization. Under either a negligible bias or a low bias condition, specifically with values lower than 0.1 eV atom$^{-1}$, the scenario can be concluded as one of soft landing, where the NCs experience no deformation upon impact, consequently generating a loosely packed porous film. As the bias is increased above this soft-landing threshold, the NCs experience a more forceful collision with the substrate, culminating in the creation of a relatively dense film.[49] On the other hand, the NCs can also be modified during the deposition process by landing on a liquid nitrogen cooled (*i.e.*, cold) substrate to further tune the crystallinity.[50]

With advancements in ultra-high vacuum (UHV) techniques, numerous enhancements have been integrated into the gas-phase condensation system, both to study NC formation and to facilitate in-flight modifications. The mass spectrometer is the most used accessory for these purposes. Both theoretical and experimental studies have shown that NCs exiting the condensation chamber typically exhibit a size distribution that follows a Gaussian profile.[2,43] As a result, incorporating a mass filter is crucial for obtaining the desired size distribution of these NCs and for selectively isolating NCs of a specific mass (size) for further processing, such as *in situ* characterization or deposition of monosized NCs onto designated substrates. Among the commonly employed mass filters for NC deposition are the quadrupole mass filter (Fig. 2a) and the time-of-flight mass filter, both of which offer significant utility in this context.[2,3,43] These mass filters can be operated in both high-resolution and low-resolution modes, thereby enabling appropriate compensation for the beam flux. The time-of-flight mass spectrometer is noted for its remarkable resolution capabilities, over an extended mass range up to $10^5$ atomic mass units (amu). On the other hand, the quadrupole mass filter exhibits a more streamlined configuration. Through a straightforward manipulation of the DC/AC voltage ratio, it can be used to effectively minimize any trade-off between flux and resolution.[51] In summary, mass spectrometers have become indispensable and are widely used, establishing themselves as standard components, in gas-phase condensation systems due to their effectiveness in analyzing and refining NC production.

As demonstrated in Fig. 3, various in-flight modifications can be incorporated along with mass-filtering when combined with UHV techniques. For instance, positioning an additional magnetron sputtering source adjacent to the NC beam allows for additional coating on the as-synthesized NCs, thereby enabling the realization of core–shell and even core–shell–shell structures in the NCs (Fig. 3a).[26] *In situ* characterization, such as time-resolved UV-vis spectroscopy (Fig. 3b),[42] small-angle X-ray scattering measurements (Fig. 3c),[52] or/and laser light scattering can also be conducted.[53] To facilitate these analyses, an appropriate window is incorporated near the sputtering source in the condensation chamber, in order to allow the transmission of light. These *in situ* measurements provide direct experimental insights into cluster formation, growth, and transport inside the condensation chamber, which could be further collaborated with numerical simulations to provide better understanding of these processes.

Gas-phase condensation offers several advantages over traditional NC synthesis methods. It provides great flexibility in material selection and the ability to simultaneously integrate multiple targets in one condensation chamber. With the use of

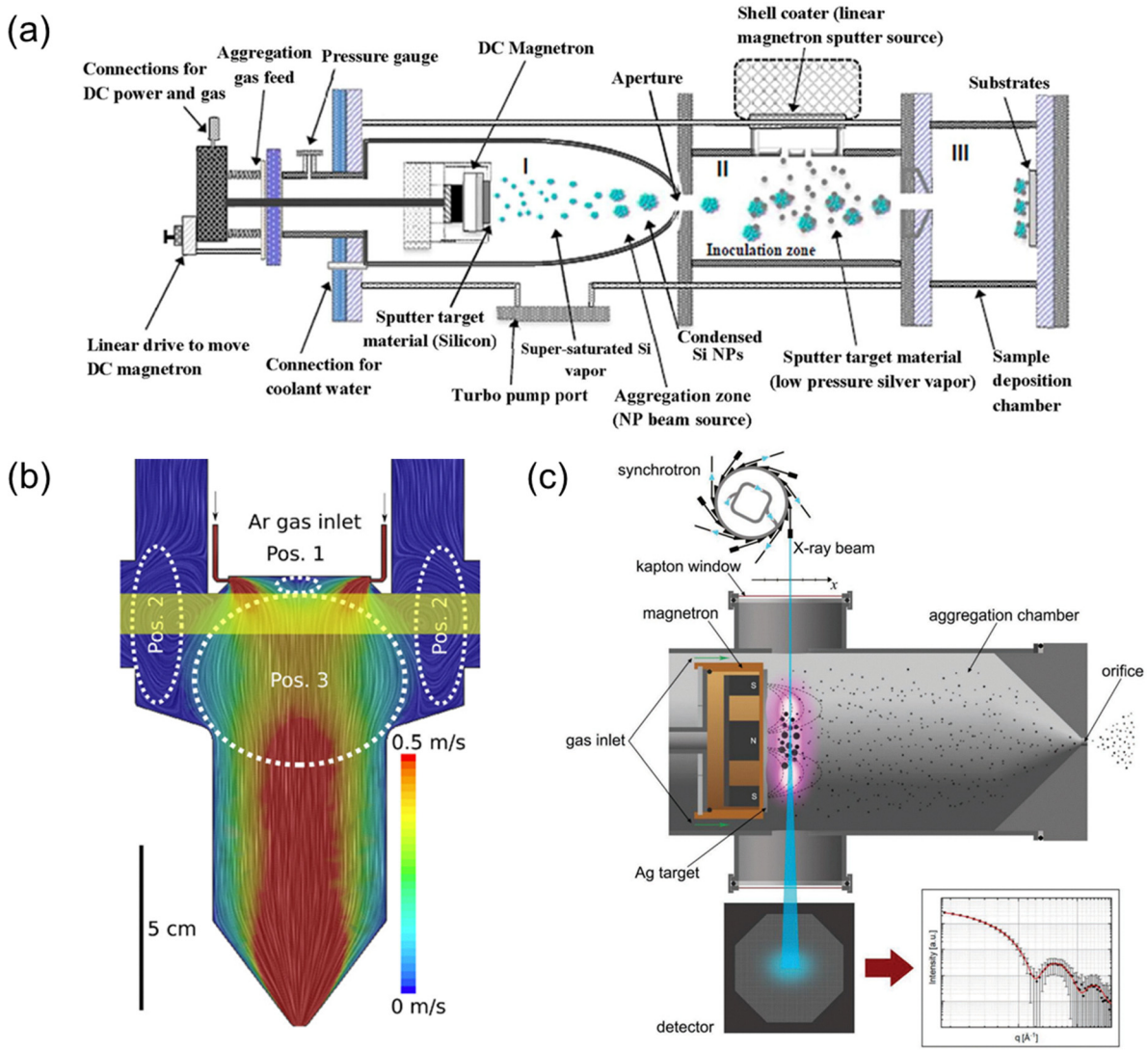


Fig. 3 (a) An additional magnetron sputtering is incorporated to provide a shell coating of the passed through NCs, to obtain core–shell NCs, such as Ag-coated Si NCs. Reproduced with permission from ref. 26. Copyright 2019, IOP Publishing Ltd. (b) A computational fluid dynamics simulation of the velocity distribution to illustrate an example of *in situ* UV-vis characterization of the assembling NCs, where the yellow region corresponds to the UV-vis beam path. Position (Pos) 1 and Pos 2 correspond to loss regions and Pos 3 corresponds to the trapping region. Reproduced with permission from ref. 42. Copyright 2021, Wiley-VCH GmbH. (c) *In situ* small angle X-ray scattering characterization of the NCs to reconstruct the scattering intensity as a function of the magnitude of the wavevector $q$ to obtain the NC size distribution by using X-ray beam from a synchrotron. Reproduced with permission from ref. 52. Copyright 2019, Wiley-VCH Verlag GmbH & Co. KGaA, Weinheim. In (b) and (c), the position of the magnetron sputtering source is movable so that the nucleation and growth of the NCs at different distances from the source can be sampled.

a DC or RF magnetron sputtering source, it can be used to generate NCs of most solid metals and metal oxides, particularly those targets with high melting points.[23–25] More importantly, this technique is capable of synthesizing NCs without using any solvents, ligands, or linkers and therefore free of any contaminant. Compared to the wet-chemistry or the hydrothermal methods, the gas-phase condensation technique also allows for more precise tuning of both the size and composition of the resulting NCs without involving complicated operation and procedures. In-flight modification, coating, and characterization can also be easily incorporated, allowing for precise growth monitoring and control over the properties of the NCs.[26] Moreover, the technique can be used with any type of substrate that can withstand low-vacuum conditions, and the substrate preparation is relatively straightforward and less time-consuming. While the gas-phase condensation technique provides a clean synthesis and direct substrate integration, the small size of NCs so produced could not take advantage of traditional structure determination (such as single-crystal X-ray diffraction) that is available to the generally larger NCs obtained by using solution-based techniques.[54] Furthermore, gas-phase deposition faces intrinsic challenges in precisely controlling interparticle distance, often leading to sintering at high coverage.[55] Nevertheless, its ability to access metastable states and enable ligand-free deposition highlights its unique potential among synthesis techniques. Overall, gas-phase

 

aggregation is a highly versatile method for producing NCs with tailored functionalities appropriate for diverse applications.

Despite these advantages in the gas-phase condensation technique, there are several limitations that could still impede the broader industrial utilization of NCs. Among these, a prominent issue is the low NC beam current.[23,27] Given the geometry of the magnetron and the buffer gas inlet, a significant proportion of the sputtered atoms undergoes redeposition onto the central target area upon post-collision with the buffer gas. Consequently, a phenomenon known as "racetrack" formation could appear on the target surface, which could significantly reduce the sputtering yield, thereby inducing inconsistency in NC production. Because only a small fraction of the NCs manages to escape from the plasma region, the dominant factor contributing to the NC loss is the effect of diffusion onto the chamber wall.[35] This is also supported by a computational fluid dynamics simulation that confirms the presence of three distinct regions where the NCs can become trapped or lost due to the influence of vortexes and drag forces, as shown in Fig. 3b.[42] The low NC beam current essentially requires extensive hours of sputtering to generate a compact NC film, which in turn deepens the erosion issue found in the sputtering target that further reduces the NC beam intensity.

Considerable advancements have been made in the last decade in enhancing the sputtering yield and ensuring consistency of the NC beam quality from its source. Increasing sputtering yield represents a direct approach to increasing the atom density of the target within the condensation chamber. Unlike the conventional planar magnetron sputtering sources, a novel hollow cathode sputtering source with a tube target could create self-sustained tube-integrated sputtering without the need for magnetic assistance, thereby substantially improving the sputtering yield and target utilization (Fig. 4a).[56] Alternatively, the development of the full-face erosion (FFE) magnetron seeks to enhance target utilization by employing movable magnets to sweep across the entire target surface (Fig. 4c).[27] This approach mitigates the low sputtering yield arising from "racetrack" formation on planar sputtering targets. Conversely, the employment of high-power impulse modes (HiPIMs) enables elevated energy levels compared to conventional DC sputtering. This causes not only an expanded influx of gas-phase atoms but also a denser plasma for seed formation, and further amplifies the NC yield (Fig. 4b).[25] Interestingly, HiPIMs exhibit differential effects on the degree of ionization of the sputtered material, thereby influencing the final NC structure, particularly in the case of bimetallic NCs. Furthermore, an innovative cluster source called the "Matrix Assembly Cluster Source" (MACS) that uses a new operating principle has been pioneered by Palmer *et al.* (Fig. 4d).[57] This source uses a cold finger mesh to condense a blend of metal atoms and buffer gas atoms into a solid germ. Cold NCs materialize after the condensed matrix is sputtered by an additional buffer gas ($Ar^+$) ion beam and they subsequently undergo deposition onto the substrate. More significantly, the MACS maintains a robust potential that can be used to scale up the cluster beam current to the milliampere level, in marked improvement to the nanoampere level obtained using the traditional gas-phase condensation technique.

## 3. Size-dependent properties of nanoclusters

The size-dependent properties of NCs are an important area of research and have significant implications for the performance

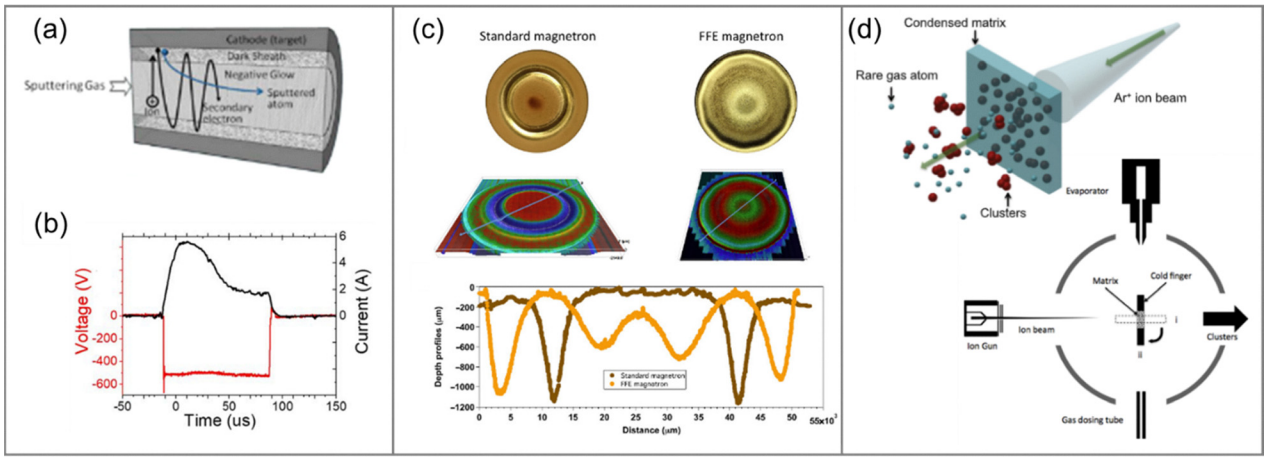


Fig. 4 (a) Magnetron sputtering source using a self-sustained hollow cathode sputtering source. Reproduced with permission from ref. 56. Copyright 2020, American Chemical Society. (b) Representative temporal pulse shape of the HiPIMs with the voltage labelled in red and the current labelled in black. Reproduced with permission from ref. 25. Copyright 2018, IOP Publishing Ltd. (c) Comparison of surface photographs (top), optical microscope images (middle) and depth profiles along the scan lines (bottom) of the sputtering targets in a standard magnetron (left) and a full-face erosion (FFE, right) magnetron. Reproduced with permission from ref. 27. Copyright 2018, Springer Nature. (d) Schematic diagrams of the concept of a Matrix Assembly Cluster Source (MACS) and the apparatus. The matrix is formed by condensing the evaporated target atoms and buffer gas atoms simultaneously onto the matrix support grid (held below 15 K by a rotatable cold finger). The resulting NCs are then deposited by sputtering the matrix with a high energy $Ar^+$ beam (set at 1 keV). Reproduced with permission from ref. 57. Copyright 2016, AIP Publishing.

of these NCs in potential applications. As outlined in the preceding section, the method used for NC synthesis could significantly affect the size, structure, and composition of the NCs so produced. Fig. 5a shows the number of publications on NCs obtained by using the gas-phase condensation technique based on a magnetron sputtering source for every five-year period since the initial development by Haberland *et al.* in 1992.[22] Between 1992 and 2004, there are only 21 publications. There is a significant surge in interest between 2010 and 2020, and a notable decline after 2020 that is likely due to constriction in experimental work during the Pandemic. We have classified these studies into four main categories of NCs: single metals, single metal oxides (*i.e.* oxides of one metal), hybrid metal/oxides (*i.e.* NCs consisting of one metal and one or more of its oxides), and multimetals. Fig. 5b shows a bar chart of the studies on these categories. Fig. 5c summarizes the elements for which the four main types of NCs synthesized by the magnetron sputtering based gas-phase condensation technique. These NC studies are compiled with short descriptions in Table S1 along with their own bibliography provided in the SI. While Fig. 5c attempts to provide a bird's eye view of the NC studies to date, Table S1 is intended to serve as a complete reference guide to these studies for researchers working in this field. Of all the reported NC studies, 55% belong to single-metal NCs, most of which can be directly synthesized by sputtering just one metal target. The noble metals are used in the majority of these single metal NC studies due to their inherent stability. There is also considerable interest in hybrid metal/oxide NCs, which consist of both metal and metal oxide NCs. Although they constitute a smaller proportion (~29%) of the studies,

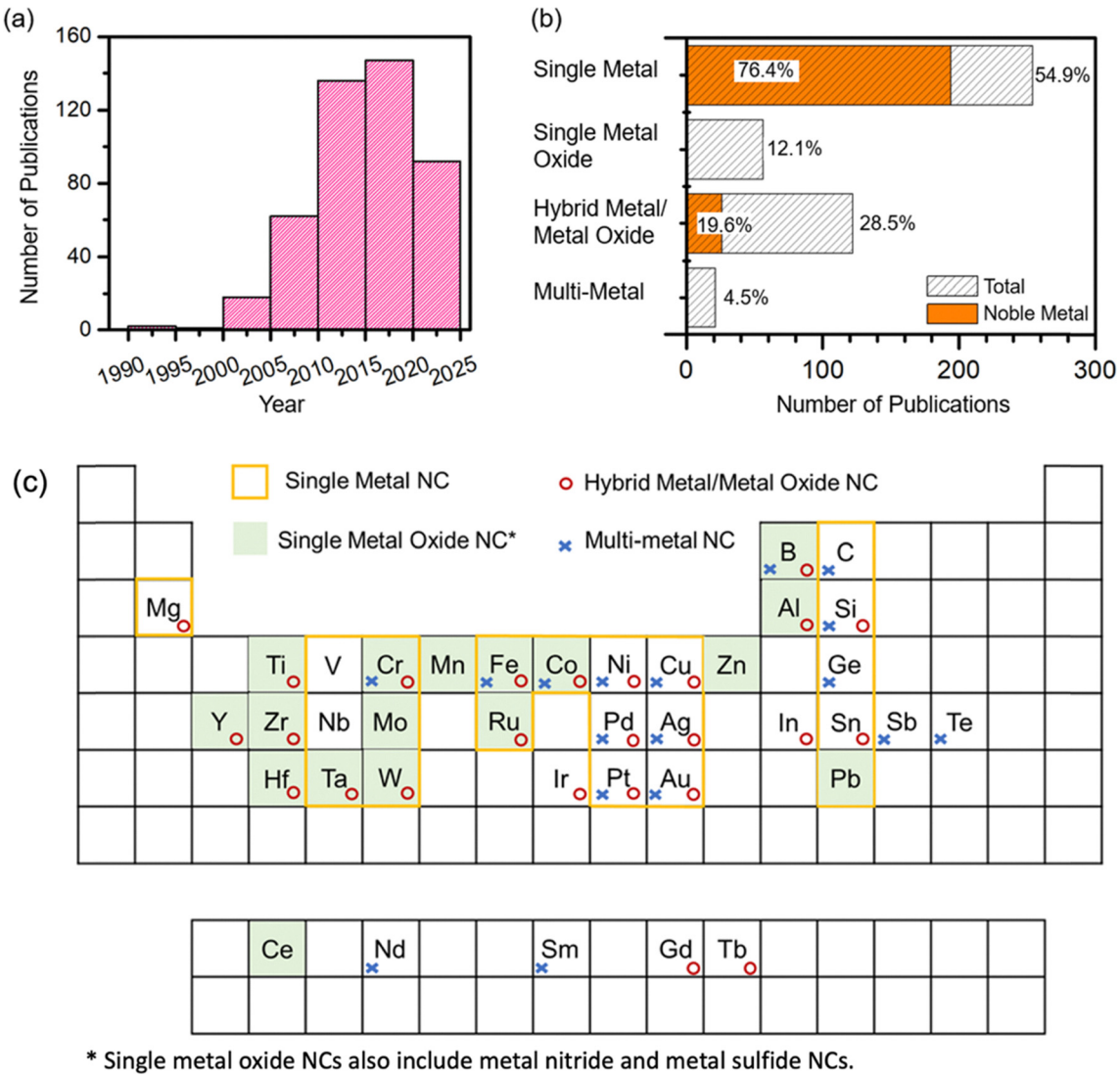


Fig. 5 (a) The number of publications of NCs synthesized by magnetron-sputtering-based gas-phase condensation technique since inception. (b) Relative distribution of studies on the four main categories of NCs: single metals, single metal oxides, hybrid metal and oxides (*i.e.*, two metal contents), and multi-metals (*i.e.*, three metal contents and above). The single metal NCs and the hybrid metal/metal oxide NCs are further sub-sectioned with noble metal and their local relative distribution in each bar graph. (c) Target materials used for the synthesis of NCs by the magnetron sputtering gas-phase condensation technique, where single metal oxide NCs also include metal nitride and metal sulfide NCs.

only 20% of which involve hybrid noble metal NCs (*i.e.* both metals in NCs are noble metals). The distribution highlights varying research focuses within the field, reflecting both the diverse applications of the NCs and the specific properties sought after in NC research. Building upon this foundation, we provide in the remaining section an overview of how these size variations intricately shape the distinctive characteristics and application performance of NCs. Unravelling the complexities of size-dependent behavior is of paramount importance, as these insights empower the researchers to meticulously engineer NCs targeted for a wide range of specific applications, from catalysis to electronics to biology, and to energy conversion. Below we explore the size-dependent structure–property–performance relations in NCs and their far-reaching implications across diverse areas of scientific inquiry and technological advancement.

Controlling the dwell time of collisions among gas-phase atoms and aggregates during the gas-phase condensation step can be used to effectively produce different size distributions of the synthesized NCs while simultaneously modifying their crystallinity and morphology. For example, ultra-small ($<10$ nm) size-selected $ZrO_2$ NCs synthesized through Zr metal NC formation followed by natural oxidation in the ambient environment exhibit an amorphous structure at 3 nm dia (in size) and start to form crystalline structures at 5 nm.[2] $TiO_2$ NCs from the same Group IV-B show a crystalline core surrounded by an amorphous shell when their size is larger than 6 nm.[4] On the other hand, amorphous $HfO_2$ is only observable in NCs below 10 nm due to surface energy relaxation. These findings suggest that a smaller grain size thermodynamically favors the formation of the amorphous phase.[58] Furthermore, Pearmain *et al.* demonstrated that Pd NCs show a notable transition from the spherical shape at 887 atoms ($\sim$3 nm) to an elongated structure at 10 000 atoms ($\sim 10 \times 20$ nm) with increasing cluster size.[59] This is due to different relaxation between cluster–cluster collisions in the condensation chamber. In addition to changes in the morphology and structure, NCs also undergo other intrinsic changes related to their size, such as variations in the melting temperature. Palmer *et al.* demonstrated that the melting point temperature of gold clusters of 2–5 nm in size is size-dependent.[60] As the temperature rises, these NCs display a coexistence of liquid on the surface and a solid core. The surface melting point decreases with smaller cluster sizes, while the core melting temperature, which is significantly higher than the surface melting point, increases as the cluster size decreases. Beyond melting, structural stability in general has also become a key focus in NC research. Modeling approaches ranging from classical to *ab initio* molecular dynamics simulations have been used to understand thermal stability behaviour and phase transitions at the nanoscale. For instance, silicon–transition metal endohedral clusters, both theoretically predicted and experimentally verified, have shown high structural stability and potential for thin-film integration.[61,62] Complementary studies using many-body GW (Green's function–screened Coulomb interaction) formalism provide a more rigorous description of electron–electron interactions, which is particularly valuable for correcting quasiparticle energy levels and predicting bandgaps, the values of which DFT often underestimates. For example, this methodology has been applied to analyze stability patterns and cohesive energy in small Si and Ge clusters, shedding light on their size-dependent optical and electronic properties.[63] Together, these observations show that structural, thermal, and phase stability in NCs are markedly different from their bulk forms. These distinctive features offer new prospects for superior performance in a wide range of applications.

Surface plasmon resonance (SPR) is a key attribute of NCs that is dynamically associated with their sizes. As the surface area of these NCs also changes accordingly with respect to their size, there is a corresponding shift in the density of surface conduction electrons, which in turn affects the resonance wavelength. This effect is particularly prominent in materials distinguished for their SPR characteristics, such as gold and silver thin films. Most NCs are found to exhibit a blue shift in the resonance frequency as their size decreases.[64] Another method of modulating the SPR involves controlling the inter-cluster spacing, which is inherently linked to particle size when maintaining the same area coverage. A decrease in inter-cluster spacing tends to result in a red shift of the NC SPR frequency.[65,66] By adjusting the size of the NCs and the spacing between them, it is therefore possible to finely tune the SPR to obtain specific optical properties, offering a versatile tool in the design of optical materials.

Due to their high surface area-to-volume ratio (or specific surface area), which results in a greater number of active sites and enhanced surface reactivity, NCs could play a vital role in surface-related applications, particularly in catalysts and sensors. While it is widely recognized that smaller NCs typically have more surface area for the same mass, thus providing potentially superior performance, it is also important to consider how the size-dependent variations in morphology, lattice structure, and chemical states could influence the catalytic efficiency of NCs. This multi-faceted impact underscores the complexity and importance of precisely controlling NC characteristics to optimize their functional performance in various applications. In most of the applications, substrates are required not only to confine the NCs to specific regions on the supports but also to enhance the charge transfer process, thereby improving performance. Since gas-phase condensation is a physical vapor deposition technique that does not depend on the nature of the substrate, a wide variety of substrates have been used for catalytic applications, including silicon, MgO powders, FTO (fluorine-doped tin oxide), and STO ($SrTiO_3$).[4,31,67,68] Additionally, interdigitated electrodes (IDEs) are commonly employed in NC sensor applications because they maximize the effective electrode length within a given device area, thereby optimizing the responsiveness and efficiency of the sensor, as illustrated in Fig. 6a.[69] These strategies demonstrate the easy adaptability of substrate integration in enhancing the functional characteristics of NCs across different applications.

In the field of hydrogen production chemistry by photoelectrochemical water splitting reaction, NCs have been extensively studied and employed for both oxygen evolution reaction (OER)

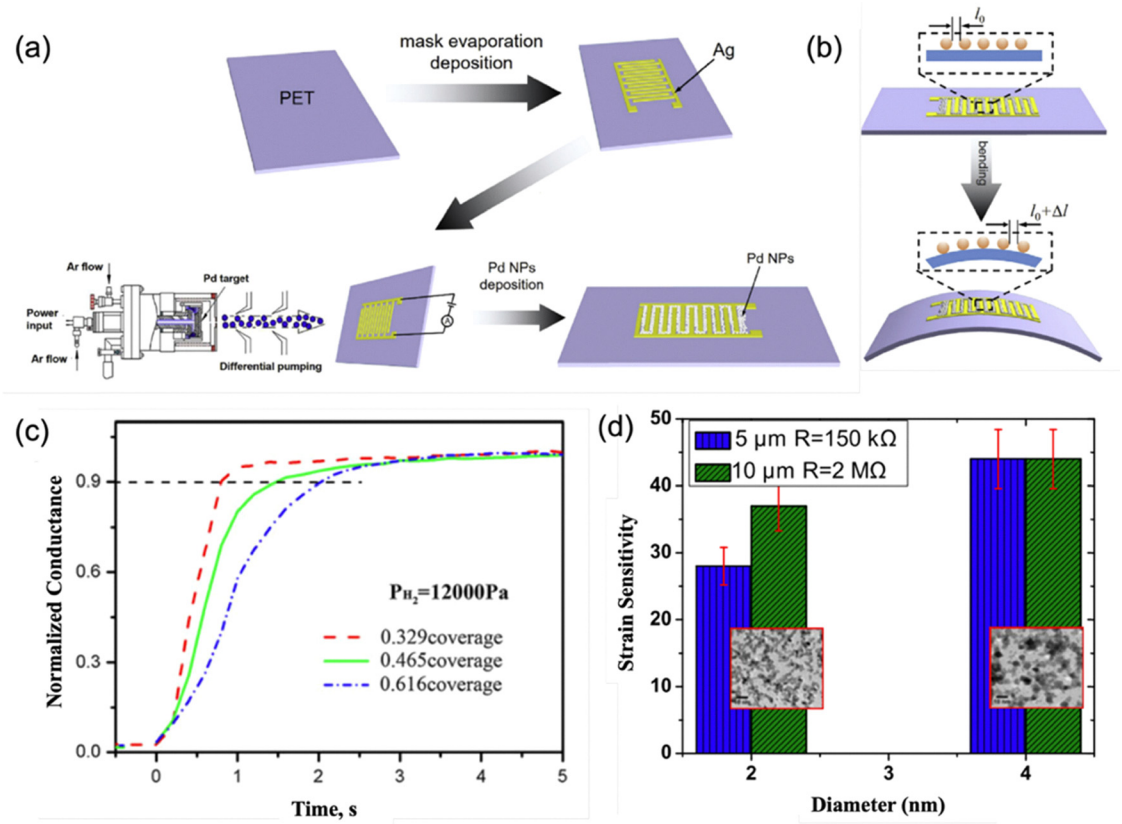


Fig. 6 (a) Schematic representation of sensor fabrication involving the creation of a silver interdigitated electrode (IDE) on a PET support followed by direct deposition of NCs onto the IDE pattern in a gas-phase condensation system. (b) Schematic diagram of sample strain measurement, where the distance between particles (*i.e.*, NCs) changes from $l_0$ to $l_0 + \Delta l$ in response to tensile strain. Reproduced with permission from ref. 69. Copyright 2018, Elsevier. (c) The size-dependent properties of NC application in gas sensors: time response profiles of the conductivity to hydrogen exposure pulses across sensor devices with different coverages of Pd NCs: red 0.329 coverage (6.1 nm), green 0.465 coverage (7.4 nm), and blue 0.616 coverage (8.6 nm). The larger NCs have more surface coverage with the same amount of NCs deposited. Reproduced with permission from ref. 70. Copyright 2013, Springer Nature. (d) The size-dependent properties of NC application in strain sensors: correlation of the strain sensitivity with the size of Pt NCs with average diameters of 2 nm and 4 nm. The size-dependency of the NCs is stronger on the IDEs with a 5 μm gap (blue) than on the IDEs with a 10 μm gap. The corresponding TEM images are shown in insets. Reproduced with permission from ref. 71. Copyright 2018, IOP Publishing Ltd.

and hydrogen evolution reaction (HER), which shows their broad functionality and versatility. NCs of transition metals and their oxides have been widely used on the OER side as photoanodes, while noble metal NCs are used for the HER as photocathodes. Strong size-dependent performance has been observed in their catalysis studies, in which NCs with smaller sizes are found to exhibit higher catalytic activities. For example, Yang *et al.* reported that the sputtering power could significantly affect the morphology and size of CoSm NCs, and the NCs with the smallest size and the highest Co concentration exhibit the highest electrocatalytic properties for the OER.[30] Additionally, our group has shown that size-selected, smaller than 6 nm $TiO_2$ NCs exhibit higher photoelectrochemical catalytic activity, shown in Fig. 7a and b,[4] while Khojasteh *et al.* demonstrated that size-selected MnO NCs with sizes of 4, 6, and 8 nm synthesized *via* gas-phase condensation exhibit enhanced catalytic activities with decreasing size.[67] On the HER side, the size-selected $Pt_n$/STO electrode exhibits enhanced electrochemical HER activity, with maximum performance found for $n$ = 30 in the range of $n$ = 1–45 between −1.35 V and −1.5 V *vs.* Ag/AgCl, as demonstrated in Fig. 7c.[68] This enhanced activity correlates with a downward shift in the LUMO level of the Pt NCs, which corresponds to their increasing size. Furthermore, Pt NCs and nanostructures are so versatile that they can be used not only as a photocathode for the HER but also as a promoter to improve the performance of other semiconductor NC photoanodes. Indeed, Srivastava *et al.* showed that introduction of Pt NC promoters could significantly reduce the number of electron–hole pairs generated in the semiconductor $TaO_x$ during the OER while efficiently enhance photoconversion.[5]

Two main origins have been identified to account for the size-dependent photocatalytic performance of NCs.[72] The first one is attributed to the so-called geometric size effect. Since photocatalysis is primarily related to reactions occurring on the surface, smaller NCs with a higher specific surface area provide more reactive sites per unit area than larger NCs when they form a monolayer on the substrate. The second one involves changes in the lattice structures and electronic states that occur with the NC size. In perfect nanocrystalline NCs, the band gap inherently increases as the NC size decreases, which could limit photon absorption (in the visible spectral region). However,

 

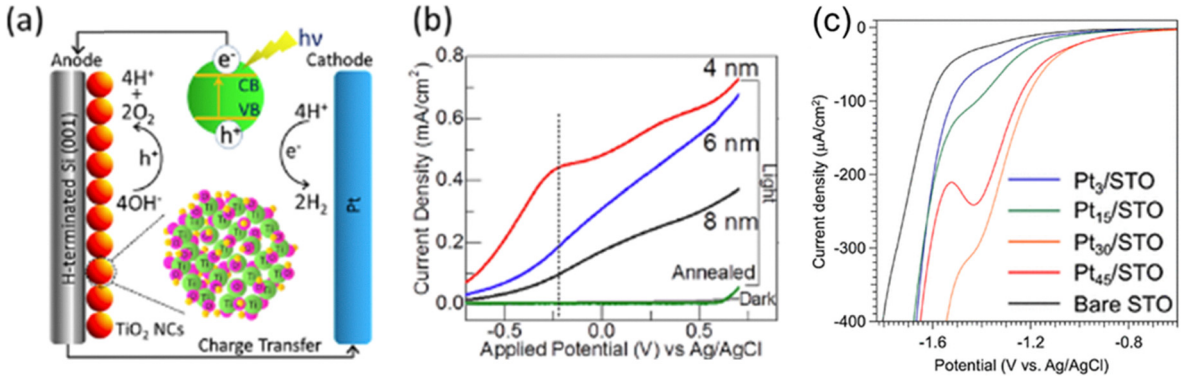


Fig. 7 (a) Schematic diagram of the mechanism of a photoelectrochemical water splitting reaction in the presence of $TiO_2$ NC catalysts. An expanded view of a $TiO_2$ NC (red spheres at the anode), consisting of Ti (green spheres), O (pink spheres), and H atoms (brown spheres), is shown as the bottom inset. The top inset shows the electron–hole pair generation in $TiO_2$ upon UV-vis light illumination, which supplies holes ($h^+$) for the oxidation of $OH^-$ leading to $O_2$ evolution at the photoanode and electrons ($e^-$), upon traveling to the counter electrode through an external circuit, for reduction leading to $H_2$ generation. (b) Photocurrent densities as a function of applied potential obtained in a photoelectrochemical water splitting reaction in a 5 M KOH electrolyte using $TiO_2$ NCs of selected sizes (4, 6 and 8 nm) and the post-annealed $TiO_2$ NCs (6 nm). The 4 nm NCs show an increased efficiency near −0.25 V, and the overall catalytic performance decreases with increasing size of NCs. Reproduced with permission from ref. 4. Copyright 2014, American Chemical Society. (c) Size-dependent electrocatalytic HER performance with different $Pt_n$ NCs on STO electrodes in a 0.1 M aqueous solution of $Na_2SO_4$. The current density of linear sweep voltammetry (LSV) curves from +0.5 V to −1.8 V (*vs.* Ag/AgCl) provide the hydrogen yield at each voltage. The $Pt_{30}$ NCs show a discernibly higher (more negative) current density compared to those for both $Pt_{15}$ and $Pt_{45}$. Reproduced with permission from ref. 68. Copyright 2018, Springer Nature.

NCs are more likely to possess higher defect concentrations compared to bulk materials. These defects introduce midgap states, consequently increasing photon absorption and enhancing the overall photocatalytic efficiency.[73] Time-dependent DFT studies, such as those by Oliveira *et al.*, have shown that optical transitions and photoabsorption spectra in NCs are highly sensitive to size and structure, offering critical insights into how electronic transitions evolve with decreasing cluster size.[74]

In addition to the photoelectrochemical water splitting reaction, NCs also provide catalytic activities for other diverse reactions. The influence of both size and composition on selectivity and efficiency is especially important to atom–atom synergies. For instance, Cai *et al.* utilized a dual target gas-phase condensation technique to synthesize Au-rich, Cu-rich, and Au/Cu-equal (with 1 : 1 composition) bimetallic NCs on agitated MgO powder.[31] Although the total sputtering powers are consistent for all the NCs, the Au/Cu-equal NCs (∼4.6 nm in size) are larger than both Au-rich and Cu-rich NCs (∼3.6 nm) due to surface agglomeration. Their study revealed that the Au/Cu-equal bimetallic NCs provide more active sites for oxygen group formation, leading to the highest catalytic reduction of 4-nitrophenol by $NaBH_4$. Additionally, Ellis *et al.* reported that PdTi NCs (5 nm in size), also produced by gas-phase condensation, exhibit excellent selectivity and efficiency for the 3-hexen-1-ol hydrogenation reaction.[75] They also showed that the NCs produced using the gas-phase condensation technique are found to provide superior performance in hydrogenation experiments compared to materials synthesized by using traditional wet chemistry methods.

Sensing represents another important broad application domain for NCs that include gas sensors,[11,70,76] DNA biosensors,[16] and strain sensors.[69,77,78] Materials such as Pd and Pt are particularly popular for use in NC-based sensors, often modified and combined with other materials such as interdigitated electrodes (IDEs) to enhance the sensitivity and selectivity. For example, Pd is extensively used in hydrogen gas detection, for which Xie *et al.* demonstrated that Pd NCs synthesized *via* gas-phase condensation with average sizes of 6.1, 7.4, and 8.6 nm could be deposited with surface coverages of 32.9%, 46.5%, and 61.6%, respectively (Fig. 6c).[70] Smaller NCs generally exhibit reduced cluster aggregation on the substrate, leading to higher exposed NC surface area and better inter-cluster gaps, which in turn enhance $H_2$ diffusion and adsorption, resulting in faster sensor response times as reflected by conductivity changes on the IDEs. In strain sensing (Fig. 6b), when Pd NCs are deposited on PET sheets patterned with IDEs, the inter-cluster spacing becomes even more crucial. Here, a single NC of a relatively larger size has more conduction electrons, and it therefore exhibits increased conductivity. As the film bends and the inter-cluster distance changes, there is a higher response current, thus enhancing sensitivity.[69] Lower surface coverage of the NCs, larger inter-cluster distance, and smaller initial resistance all contribute to the higher sensitivity and greater differentiation. These studies show that the sensitivity of the NC sensors can be adjusted by tuning the NC deposition process. When Pt NCs are used in strain sensing applications, they exhibit higher sensitivity compared to Pd NCs, with a 4 nm Pt NC film (Fig. 6d) reaching a sensitivity comparable to an 8.2 nm Pd NC film (shown in Fig. 6a of ref. 69).[69,71] Similarly, the larger NCs with greater inter-cluster spacings also yield higher sensitivity. Overall, while sensing applications are primarily influenced by the surface chemical states of the material, the achievable sensitivity also depends on the inter-cluster spacings of the NCs on the substrate. Although smaller NCs may offer larger specific surface areas

for increased contact points, overly close NCs with small inter-cluster spacing could hinder gas diffusion or mechanical movement detection. Both cluster size and inter-cluster spacing are therefore critical parameters that should be carefully adjusted during deposition to optimize sensor sensitivity.

NCs with varying sizes could give rise to novel phases and defects with different locations and compositions that could also have a significant impact on spin alignment within the NCs, particularly in the context of defects resulting from surface oxidation in transition metal oxide NCs. Early density functional theory (DFT) studies have shown that oxygen vacancy defects in $ZrO_2$ NCs are more likely to form at low coordination sites such as corners and edges.[79] Therefore, the number and type of oxygen vacancy defects could change depending on the size of the $ZrO_2$ NCs. The presence of these defects also stabilizes the tetragonal structure of $ZrO_2$ NCs at room temperature, in notable contrast to the monoclinic phase as the most stable structure found for bulk $ZrO_2$.[2,80] As illustrated in Fig. 8b, in tetragonal $ZrO_2$ NCs, a single oxygen atom can trigger the reduction of four nearby $Zr^{4+}$ ions to $Zr^{3+}$ ions, forming a resonance structure. The electron hopping between the $Zr^{3+}$ ion and the singly charged oxygen vacancy favors spin splitting and ferromagnetic alignment, in marked contrast to bulk $ZrO_2$, which is diamagnetic. This work also shows that ferromagnetism in $ZrO_2$ NCs is size-dependent (Fig. 8a), which is also related to the surface defect concentration. This behavior suggests that another approach to manipulating the magnetic performance is by means of size control. Similarly, the NCs of $HfO_2$, another Group IV-B metal oxide, obtained by gas-phase condensation have also been reported to have a mixture of tetragonal and monoclinic structures that exhibit paramagnetism.[81] These dopant-free, ligand-free transition metal oxide NCs are strong material candidates for the next generation spintronics.[82]

Other remarkable performances in biology, energy storage, and electrical device applications have also been demonstrated for NCs obtained by the gas-phase condensation technique without delving too much into their size-dependency. Mery *et al.* demonstrated that there is a significant change in both density and morphological effect for cell spreading onto sterile glass covers decorated with Ag NCs.[83] The cells appear to change from their typically expanded morphology to a spherical one. Surprisingly, no toxicity has been found for those Ag NCs. In the field of energy storage, the efficiency of $H_2$ storage in Mg films can be significantly enhanced by depositing Pd NCs onto a Mg thin film.[84] Their DFT study also revealed that the transformation of cubic Pd into a hexagonal structure near the interface is governed by interfacial strain. Furthermore, the

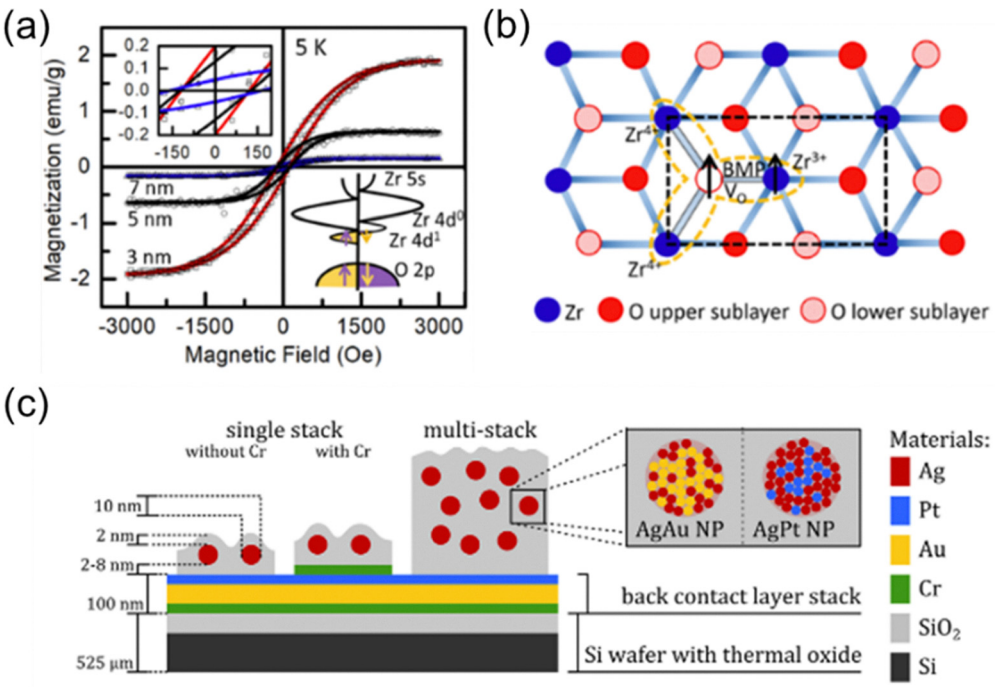


Fig. 8 (a) Measured (symbols) and fitted ferromagnetic hysteresis loops (solid lines) of as-grown $ZrO_2$ NCs of different sizes obtained at 5 K. The right bottom inset presents the band-splitting leading to ferromagnetism generation: an impurity band contributed by Zr $4d_1$ ($Zr^{3+}$) is caused by the oxygen vacancy defects. This impurity band could merge and hybridize with the conduction band, which triggers band-splitting into spin-up and spin-down states. (b) Schematic presentation of the formation of magnetic polarons in an unreconstructed $ZrO_2$ (1 0 1) surface. The missing oxygen vacancy ($V_O$) in the lower sublayer triggers four nearby Zr ions (the one below $V_O$ is not shown) with two excess electrons. The electron trapping in the oxygen vacancy could couple with the other electron located in $Zr^{3+}$ *via* exchange interaction, generating the magnetic polaron. Reproduced with permission from ref. 2. Copyright 2020, American Chemical Society. (c) Schematic depiction of a typical setup of NC-based memristor. For a detailed assessment of memristive behaviour of single NCs, single stack $SiO_2$/NC/$SiO_2$ devices (with and without an additional Cr wetting layer) are characterized by conductive atomic force microscopy. Reproduced with permission from ref. 88. Copyright 2019, Springer Nature.

study indicated that prior hydrogen saturation of the Pd NCs increases their nanoportal efficiency. Another area of application for NCs is memristors, which are two-terminal non-volatile memory devices that can maintain their resistance state based on the voltage bias applied on and the current passing through them.[85,86] Their memory capabilities, low power consumption, and scalability make them attractive for a variety of applications, including artificial intelligence, neuromorphic computing, data storage, and energy-efficient electronics.[87] Building on these insights, Vahl *et al.* successfully used the gas-phase condensation technique to embed bimetallic NCs (11 nm AgAu or 9 nm AgPt NCs) into a $SiO_2$ dielectric matrix, forming a vertically sandwiched two-terminal device, shown in Fig. 8c.[88] This device exhibits a reliable pinched current–voltage hysteresis loop at the level of individual NCs, without requiring any additional electroforming step. Moreover, networks of atomic clusters have been reported to serve as architectures for neuromorphic computing systems, where the formation and breakage of connections between clusters mimic synaptic behaviors.[89]

These findings show that the relevance of NCs in memristive and neuromorphic applications comes not only from their small size and scalability, but also from the high level of control in their synthesis and the tunability of their properties. The ability to fine-tune NC composition and structure allows researchers to explore diverse functions and device architectures. These studies utilizing ultra-small NCs illustrate their immense potential for revolutionary applications spanning catalysis, electronics, medicine, and beyond. Leveraging the inherent advantages of precise size manipulation facilitated by the gas-phase condensation technique coupled with mass selection, the performance of NCs can be further optimized through meticulous size-dependent investigations.

## 4. Conclusions and outlook

NCs represent a novel class of advanced materials with a fascinating size regime in between individual atoms and bulk materials. The size of the NC plays a crucial role in controlling, among other properties, the specific surface area, electron orbital merging, and defect formation. In this context, the gas-phase condensation technique stands out as a powerful and versatile method for synthesizing NCs with tailored properties and controllable size distributions. This bottom-up approach allows precise control over seed nucleation in the gas phase, cluster growth by aggregation, and soft landing onto a substrate, while facilitating the production of ''high-purity'' NCs with unique structures and enhanced functionalities. The magnetron sputtering source enables a wide selection of NC materials. The integration of other ultra-high vacuum techniques allows comprehensive in-flight modifications and *in situ* characterization of NCs of different sizes. The interplay of geometric size effects, quantum confinement, and defects collaboratively influences the performance of NCs in a broad spectrum of applications, spanning from catalysis to sensing, to nanoelectronics and memristive devices and beyond.

There remain several limitations that could hinder the extensive industrial adoption of NCs created by the gas-phase condensation technique. These challenges are a low target utilization rate, limited NC yield, and beam current constraints. Dedicated efforts have been devoted to improving the source technology to establish a high-yield source with a long-term stability while simultaneously accommodating the diverse array of NC generation requirements. Given the remarkable performance demonstrated by NCs across a wide range of applications, there is a continued strong interest in understanding the size-dependent properties and phenomena of NCs containing multiple metals and metal oxides. In these more intricate NCs, their composition introduces an additional dimension of control over defects and bands that could deeply affect their performance metrics. Embarking on an exploration of size-dependent applications in NCs, researchers devote themselves to a dynamic and sophisticated venture fueled by cutting-edge research, sophisticated materials synthesis methodologies, and advanced computational simulations. This multidisciplinary pursuit is continually evolving with the collective goal to unlock the vast potential of NCs.

## Conflicts of interest

There are no conflicts to declare.

## Data availability

As this is a review article, no primary research results, software or code were included. No new data were generated or analysed as part of this review.

Supplementary information (SI): summary of studies published to date (2024) on NCs obtained by using magnetron-sputtering based gas-phase condensation technique, along with their bibliography. See DOI: https://doi.org/10.1039/d5cc07296d.

## Acknowledgements

This work was supported by the Natural Sciences and Engineering Research Council of Canada.

## References

1 W. G. Kreyling, M. Semmler-Behnke and Q. Chaudhry, *Nano Today*, 2010, **5**, 165–168.
2 X. Guan, S. Srivastava, J. P. Thomas, N. F. Heinig, J. S. Kang, M. A. Rahman and K. T. Leung, *ACS Appl. Mater. Interfaces*, 2020, **12**, 48998–49005.
3 R. E. Palmer, S. Pratontep and H.-G. Boyen, *Nat. Mater.*, 2003, **2**, 443–448.
4 S. Srivastava, J. P. Thomas, M. A. Rahman, N. F. Heinig and K. T. Leung, *ACS Nano*, 2014, **8**, 11891–11898.
5 S. Srivastava, J. P. Thomas, N. Heinig, M. Abd-Ellah, M. A. Rahman and K. T. Leung, *Nanoscale*, 2017, **9**, 14395–14404.
6 S. Kalita, R. Kandimalla, A. C. Bhowal, J. Kotoky and S. Kundu, *Sci. Rep.*, 2018, **8**, 5778.
7 L. Gong, H. Kuai, S. Ren, X. H. Zhao, S. Y. Huan, X. B. Zhang and W. Tan, *Chem. Commun.*, 2015, **51**, 12095–12098.
8 J. Zhang, K. Sasaki, E. Sutter and R. R. Adzic, *Science*, 2007, **315**, 220–222.

9 K. Vamvakidis, S. Mourdikoudis, A. Makridis, E. Paulidou, M. Angelakeris and C. Dendrinou-Samara, *J. Colloid Interface Sci.*, 2018, **511**, 101–109.
10 E. Skotadis, E. Aslanidis, M. Kainourgiaki and D. Tsoukalas, *Appl. Nano*, 2020, **1**, 70–86.
11 E. Skotadis, J. L. Tanner, S. Stathopoulos, V. Tsouti and D. Tsoukalas, *Sens. Actuators, B*, 2012, **175**, 85–91.
12 E. Skotadis, G. Tsekenis, M. Chatzipetrou, L. Patsiouras, L. Madianos, P. Bousoulas, I. Zergioti and D. Tsoukalas, *Sens. Actuators, B*, 2017, **239**, 962–969.
13 Y. Liu, D. Yao and H. Zhang, *ACS Appl. Mater. Interfaces*, 2018, **10**, 12071–12080.
14 N. Carstens, B. Adejube, T. Strunskus, F. Faupel, S. Brown and A. Vahl, *Nanoscale Adv.*, 2022, **4**, 3149–3160.
15 G. Yin, M. Nishikawa, Y. Nosaka, N. Srinivasan, D. Atarashi, E. Sakai and M. Miyauchi, *ACS Nano*, 2015, **9**, 2111–2119.
16 E. Skotadis, K. Voutyras, M. Chatzipetrou, G. Tsekenis, L. Patsiouras, L. Madianos, S. Chatzandroulis, I. Zergioti and D. Tsoukalas, *Biosens. Bioelectron.*, 2016, **81**, 388–394.
17 K. Liao, P. Mao, Y. Li, Y. Nan, F. Song, G. Wang and M. Han, *Sens. Actuators, B*, 2013, **181**, 125–129.
18 B. Xie, S. Zhang, F. Liu, X. Peng, F. Song, G. Wang and M. Han, *Sens. Actuators, A*, 2012, **181**, 20–24.
19 W. W. Gerberich, J. M. Jungk and W. M. Mook, The Bottom-up Approach to Materials by Design, in *Nano and Microstructural Design of Advanced Materials*, 2003, vol. Commemorative, pp. 211–220.
20 D. Kim, H. S. Kim, S. M. Park, M. J. Ji, B. H. Choi and M. Kang, *J. Ind. Eng. Chem.*, 2014, **20**, 505–511.
21 S. Srivastava, J. P. Thomas, N. F. Heinig and K. T. Leung, *ACS Appl. Mater. Interfaces*, 2017, **9**, 36989–36996.
22 H. Haberland, M. Karrais, M. Mall and Y. Thurner, *J. Vac. Sci. Technol., A*, 1992, **10**, 3266–3271.
23 O. Kylián, D. Nikitin, J. Hanuš, S. Ali-Ogly, P. Pleskunov and H. Biederman, *J. Vac. Sci. Technol., A*, 2023, **41**, 020802.
24 O. Polonskyi, A. M. Ahadi, T. Peter, K. Fujioka, J. W. Abraham, E. Vasiliauskaite, A. Hinz, T. Strunskus, S. Wolf, M. Bonitz, H. Kersten and F. Faupel, *Eur. Phys. J. D*, 2018, **72**, 93.
25 A. Mayoral, L. Martínez, J. M. García-Martín, I. Fernández-Martínez, M. García-Hernández, B. Galiana, C. Ballesteros and Y. Huttel, *Nanotechnol.*, 2018, **30**, 065606.
26 O. Kylián, R. Štefaníková, A. Kuzminova, J. Hanuš, P. Solař, P. Kúš, M. Cieslar and H. Biederman, *Plasma Phys. Controlled Fusion*, 2020, **62**, 014005.
27 Y. Huttel, L. Martínez, A. Mayoral and I. Fernández, *MRS Commun.*, 2018, **8**, 947–954.
28 A. Kusior, K. Kollbek, K. Kowalski, M. Borysiewicz, T. Wojciechowski, A. Adamczyk, A. Trenczek-Zajac, M. Radecka and K. Zakrzewska, *Appl. Surf. Sci.*, 2016, **380**, 193–202.
29 C. Binns, in *Handbook of Metal Physics*, ed. J. A. Blackman, Elsevier, 2008, vol. 5, pp. 49–71.
30 Y. Yang, Y. Li, H. Luo, C. Song, J. Huang, Z. Dong, J. Wu, Y. Li, F. Meng and J. Zhang, *Mater. Today Commun.*, 2023, **35**, 106240.
31 R. Cai, P. R. Ellis, J. Yin, J. Liu, C. M. Brown, R. Griffin, G. Chang, D. Yang, J. Ren, K. Cooke, P. T. Bishop, W. Theis and R. E. Palmer, *Small*, 2018, **14**, 1703734.
32 L. Martínez, M. Díaz, E. Román, M. Ruano, D. Llamosa P. and Y. Huttel, *Langmuir*, 2012, **28**, 11241–11249.
33 S. Al Khabouri, S. Al Harthi, T. Maekawa, M. E. Elzain, H. H. Kyaw, M. T. Zar Myint and K. Laxman, *Mater. Chem. Phys.*, 2021, **271**, 124858.
34 A. I. Ayesh, *J. Alloys Compd.*, 2018, **745**, 299–305.
35 L. Zhang, J. Shao and X. Chen, *Vacuum*, 2016, **128**, 137–145.
36 H. Haberland, P. Melinon, J. A. De Toro, P. S. Normile and C. Binns, in *Gas-Phase Synthesis of Nanoparticles*, ed. Y. Huttel, Wiley-VCH Verlag GmbH & Co. KGaA, 2018, pp. 1–56.
37 F. Baletto, C. Mottet and R. Ferrando, *Phys. Rev. B: Condens. Matter Mater. Phys.*, 2001, **63**, 155408.
38 C. Cassidy, V. Singh, P. Grammatikopoulos, F. Djurabekova, K. Nordlund and M. Sowwan, *Sci. Rep.*, 2018, **3**, 3083.
39 V. Singh, C. Cassidy, P. Grammatikopoulos, F. Djurabekova, K. Nordlund and M. Sowwan, *J. Phys. Chem. C*, 2014, **118**, 13869–13875.
40 M. Bohra, P. Grammatikopoulos, V. Singh, J. Zhao, E. Toulkeridou, S. Steinhauer, J. Kioseoglou, J. F. Bobo, K. Nordlund, F. Djurabekova and M. Sowwan, *Phys. Rev. Mater.*, 2017, **1**, 066001.
41 J. Zhao, E. Baibuz, J. Vernieres, P. Grammatikopoulos, V. Jansson, M. Nagel, S. Steinhauer, M. Sowwan, A. Kuronen, K. Nordlund and F. Djurabekova, *ACS Nano*, 2016, **10**, 4684–4694.
42 J. Drewes, S. Ali-Ogly, T. Strunskus, O. Polonskyi, H. Biederman, F. Faupel and A. Vahl, *Plasma Processes Polym.*, 2022, **19**, 1–11.
43 Y. Xia, D. Nelli, R. Ferrando, J. Yuan and Z. Y. Li, *Nat. Commun.*, 2021, **12**, 1–8.
44 A. M. Ahadi, V. Zaporojtchenko, T. Peter, O. Polonskyi, T. Strunskus and F. Faupel, *J. Nanopart. Res.*, 2013, **15**, 2125.
45 J. Zhao, A. Mayoral, L. Martínez, M. P. Johansson, F. Djurabekova and Y. Huttel, *J. Phys. Chem. C*, 2020, **124**, 24441–24450.
46 P. Grammatikopoulos, S. Steinhauer, J. Vernieres, V. Singh and M. Sowwan, *Adv. Phys.: X*, 2016, **1**, 81–100.
47 V. N. Popok, *Mater. Sci. Eng., R*, 2011, **72**, 137–157.
48 H. Haberland, Z. Insepov and M. Michael, *Phys. Rev. B: Condens. Matter Mater. Phys.*, 1995, **51**, 11061–11067.
49 V. N. Popok, I. Barke, E. E. B. Campbell and K. H. Meiwes-Broer, *Surf. Sci. Rep.*, 2011, **66**, 347–377.
50 Y. M. Sung, J. S. Park and T. G. Kim, *J. Non-Cryst. Solids: X*, 2012, **358**, 182–187.
51 V. N. Popok and L. Gurevich, *J. Nanopart. Res.*, 2019, **21**, 1–9.
52 A. Shelemin, P. Pleskunov, J. Kousal, J. Drewes, J. Hanuš, S. Ali-Ogly, D. Nikitin, P. Solař, J. Kratochvíl, M. Vaidulych, M. Schwartzkopf, O. Kylián, O. Polonskyi, T. Strunskus, F. Faupel, S. V. Roth, H. Biederman and A. Choukourov, *Part. Part. Syst. Charact.*, 2020, **37**, 1900436.
53 J. Drewes, S. Rehders, T. Strunskus, H. Kersten, F. Faupel and A. Vahl, *Part. Part. Syst. Charact.*, 2022, **39**, 2200112.
54 Y. Du, H. Sheng, D. Astruc and M. Zhu, *Chem. Rev.*, 2020, **120**, 526–622.
55 M. Gracia-Pinilla, E. Martínez, G. S. Vidaurri and E. Pérez-Tijerina, *Nanoscale Res. Lett.*, 2010, **5**, 180–188.
56 J. Liu, S. H. He and J. P. Wang, *ACS Appl. Nano Mater.*, 2020, **3**, 7942–7949.
57 R. E. Palmer, L. Cao and F. Yin, *Rev. Sci. Instrum.*, 2016, **87**, 046103.
58 G. Sharma, S. V. Ushakov, H. Li, R. H. R. Castro and A. Navrotsky, *J. Phys. Chem. C*, 2017, **121**, 10392–10397.
59 D. Pearmain, S. J. Park, A. Abdela, R. E. Palmer and Z. Y. Li, *Nanoscale*, 2015, **7**, 19647–19652.
60 D. M. Foster, T. Pavloudis, J. Kioseoglou and R. E. Palmer, *Nat. Commun.*, 2019, **10**, 2583.
61 G. K. Gueorguiev, J. M. Pacheco, S. Stafström and L. Hultman, *Thin Solid Films*, 2006, **515**, 1192–1196.
62 J. M. Pacheco, G. K. Gueorguiev and J. L. Martins, *Phys. Rev. B: Condens. Matter Mater. Phys.*, 2002, **66**, 334011–334013.
63 M. I. A. Oliveira, R. Rivelino, F. De Brito Mota and G. K. Gueorguiev, *J. Phys. Chem. C*, 2014, **118**, 5501–5509.
64 S. Palomba, L. Novotny and R. E. Palmer, *Opt. Commun.*, 2008, **281**, 480–483.
65 Y. Gong, Y. Zhou, L. He, B. Xie, F. Song, M. Han and G. Wang, *Eur. Phys. J. D*, 2013, **67**, 87.
66 L. B. He, Y. L. Wang, X. Xie, M. Han, F. Q. Song, B. J. Wang, W. L. Chen, H. X. Xu and L. T. Sun, *Phys. Chem. Chem. Phys.*, 2017, **19**, 5091–5101.
67 M. Khojasteh, S. Haghighat, J. M. Dawlaty and V. V. Kresin, *Nanotechnol.*, 2018, **29**, 215603.
68 H. Tsunoyama, Y. Yamano, C. Zhang, M. Komori, T. Eguchi and A. Nakajima, *Top. Catal.*, 2018, **61**, 126–135.
69 B. Xie, P. Mao, M. Chen, Z. Li, C. Liu, Y. Qin, L. Yang, M. Wei, M. Liu, X. Wang, D. Han, S. Li, F. Song, M. Han, J. M. Liu and G. Wang, *Sens. Actuators, A*, 2018, **272**, 161–169.
70 B. Xie, M. Zheng, F. Liu, X. Peng, G. Wang and M. Han, *J. Nanopart. Res.*, 2013, **15**, 1746.
71 L. Patsiouras, E. Skotadis, N. Gialama, C. Drivas, S. Kennou, K. Giannakopoulos and D. Tsoukalas, *Nanotechnol.*, 2018, **29**, 465706.
72 Y. Iwasawa, K. Asakura and M. Tada, in *XAFS Techniques for Catalysts, Nanomaterials, and Surfaces*, ed. Y. Iwasawa, K. Asakura and M. Tada, Springer Nature, Switzerland, 1st edn, 2017, pp. 273–298.
73 M. A. Rahman, J. P. Thomas and K. T. Leung, *Adv. Energy Mater.*, 2018, **8**, 1701234.
74 M. J. T. Oliveira, P. V. C. Medeiros, J. R. F. Sousa, F. Nogueira and G. K. Gueorguiev, *J. Phys. Chem. C*, 2014, **118**, 11377–11384.
75 P. R. Ellis, C. M. Brown, P. T. Bishop, J. Yin, K. Cooke, W. D. Terry, J. Liu, F. Yin and R. E. Palmer, *Faraday Discuss.*, 2016, **188**, 39–56.

 

76 M. Chen, P. Mao, Y. Qin, J. Wang, B. Xie, X. Wang, D. Han, G. H. Wang, F. Song, M. Han, J. M. Liu and G. Wang, *ACS Appl. Mater. Interfaces*, 2017, **9**, 27193–27201.
77 E. Aslanidis, E. Skotadis, E. Moutoulas and D. Tsoukalas, *Sensors*, 2020, **20**, 2584.
78 J. L. Tanner, D. Mousadakos, K. Giannakopoulos, E. Skotadis and D. Tsoukalas, *Nanotechnol.*, 2012, **23**, 285501.
79 E. Albanese, A. Ruiz Puigdollers and G. Pacchioni, *ACS Omega*, 2018, **3**, 5301–5307.
80 S. Ning, P. Zhan, Q. Xie, Z. Li and Z. Zhang, *J. Phys. D: Appl. Phys.*, 2013, **46**, 445004.
81 K. Q. Lin, L. Sen Wang, Z. W. Wang, R. T. Wen, Y. Chen and D. L. Peng, *Eur. Phys. J. D*, 2013, **67**, 42.
82 S. B. Ogale, *Adv. Mater.*, 2010, **22**, 3125–3155.
83 M. Mery, N. Orellana, C. A. Acevedo, S. Oyarzún, F. Araneda, G. Herrera, D. Aliaga, W. Creixell, T. P. Corrales and C. P. Romero, *Materials*, 2018, **11**, 2574.
84 S. Kumar, T. Pavloudis, V. Singh, H. Nguyen, S. Steinhauer, C. Pursell, B. Clemens, J. Kioseoglou, P. Grammatikopoulos and M. Sowwan, *Adv. Energy Mater.*, 2018, **8**, 1701326.
85 L. O. Chua, *IEEE Trans. Circuit Theory*, 1971, **18**, 507–519.
86 D. B. Strukov, G. S. Snider, D. R. Stewart and R. S. Williams, *Nature*, 2008, **453**, 80–83.
87 I. H. Im, S. J. Kim and H. W. Jang, *Adv. Intell. Syst.*, 2020, **2**, 2000105.
88 A. Vahl, N. Carstens, T. Strunskus, F. Faupel and A. Hassanien, *Sci. Rep.*, 2019, **9**, 17367.
89 W. Wu, A. V. Verkhovtsev, T. Pavloudis, A. V. Solov'yov and R. E. Palmer, *Nano Res.*, 2023, **16**, 10500–10506.